
Article:
Zhang, Y., Bai, J., Guo, K. et al. (2025) Enhanced magnetocaloric effect in Ni-Mn-Sn alloys by synergistic manipulation of magnetization difference and lattice volume. Applied Materials Today, 42. 102589. ISSN: 2352-9407

https://doi.org/10.1016/j.apmt.2025.102589

Enhanced magnetocaloric effect in Ni-Mn-Sn alloys by synergistic manipulation of magnetization difference and lattice volume

Yu Zhang[1,2], Jing Bai[1,2,*], Keliang Guo[1], Dan Liu[1,2], Yansong Li[1,2], Jianglong Gu[3], Qingshuang Ma[2], Qiuzhi Gao[2], Nicola Morley[4], Liang Zuo[1]

[1]Key Laboratory for Anisotropy and Texture of Materials (Ministry of Education), School of Material Science and Engineering, Northeastern University, Shenyang 110819, China

[2]Key Laboratory of Dielectric and Electrolyte Functional Material Hebei Province, School of Resources and Materials, Northeastern University at Qinhuangdao, Qinhuangdao 066004, PR China

[3]State Key Laboratory of Metastable Materials Science and Technology, Yanshan University, Qinhuangdao 066004, China

[4]Department of Material Science and Engineering, University of Sheffield, Sheffield, S1 3JD, UK

*Corresponding author: Jing Bai: baijing@neuq.edu.cn

Abstract

Ni-Mn-based alloys are renowned for their outstanding magnetocaloric effect, attributed to their significant magnetization difference ($\triangle M$) and low thermal hysteresis (ΔT_{hys}) during magneto-structural transition. This study employs first-principles calculations to explore the martensitic transformation, magnetic properties, and electronic structure of the Co doped $Ni_{2-x}Co_xMn_{1.5}Sn_{0.5}$ (x = 0–0.42) alloys. The results show that Co tends to directly occupy the Ni sublattice, and the volumes of ferromagnetic austenite and ferrimagnetic six-layer modulated (6M) and non-modulated (NM) martensites decrease with increasing Co content due to the strong bonding and interaction between Co atoms and surrounding atoms. The possible phase transformation sequence including the complex structure 6M martensite was clarified. From the perspective of phase transformation driving force, the fundamental reason why the martensitic transformation temperature decreases with the increase of Co content is explained. It also clarifies the composition range of magneto-structural coupling is $0.25 \leq x < 0.33$. Furthermore, the physical properties of Si-doped $Ni_{1.75}Co_{0.25}Mn_{1.5}Sn_{0.5}$ alloy with a large $\triangle M$ of 4.59 μ_B/f.u. were also studied. The results show that Si atoms preferentially occupy the Mn_{Sn} sublattice, and Si doping can enhance the phase stability of austenite, 6M and NM martensites, reduce the tetragonal distortion and volume change during the martensitic transformation, and thus

may have the benefit to reduce ΔT_{hys}. These findings provide foundational insights for designing new alloys with improved properties.

Keywords: Ni-Mn-Sn-Co-(Si), first-principles calculations, martensitic transformation, magnetism, 6M martensite

1 Introduction

Magnetic refrigeration technology based on the magnetocaloric effect (MCE) has emerged as the leading candidate to replace traditional vapor compression refrigeration. Among various magnetic refrigeration materials, Ni-Mn-based magnetic shape memory alloys (MSMAs) stand out due to their eco-friendliness, energy efficiency, and cost-effectiveness, addressing the pressing challenges of ozone depletion and global warming. The multifunctional properties of these alloys can be controlled through the application of an external magnetic field, including the magnetic shape memory effect (MSME)[1,2], magnetoresistance (MR)[3-5], and MCE[6-8]. These effects are closely associated with martensitic transformation, characterized by coupled changes in structure and magnetization, transitioning from ferromagnetic austenite to weakly magnetic martensite. Consequently, these alloys hold significant potential as candidate materials for various applications, including actuators, sensors, and solid-state magnetic refrigeration systems[9-11]. In particular, Ni-Mn-Sn alloy does not contain expensive elements such as Ga and In, so its raw material cost is much lower than Ni-Mn-Ga and Ni-Mn-In based alloys, making it more attractive for large-scale practical applications.

Ni-Mn-Sn alloy, which capitalizes on the latent heat associated with magneto-structural transition[6] to achieve significant MCE. This magnetic transition is driven by Zeeman energy $E_{zeeman}=\mu_0 H\triangle M$, with $\triangle M$ representing the difference in magnetization between the martensite and austenite, and H standing for the applied magnetic field. Therefore, a larger $\triangle M$ aids in obtaining a stronger driving force during the magnetic transition, which is a prerequisite for MSMAs to exhibit their unique functional properties. However, thermal hysteresis (ΔT_{hys}), an inherent attribute of magnetic structural transitions, remains a detrimental factor that directly affects the cooling capacity and reversibility of the MCE. To enhance the performance of magnetocaloric materials, this adverse effect should be minimized. From the perspective of developing high-performance magnetocaloric materials, a higher $\triangle M$ and lower ΔT_{hys} are highly desirable characteristics.

Alloying is an effective method to adjust properties related to magneto-structural transition, such as martensitic transformation temperature, Curie temperature, magnetization difference, thermal hysteresis, and entropy change[1,12,13]. Researchers have found that the magnetization differences in Co-doped $Ni_{43}Co_7Mn_{38.8}Sn_{11.2}$[14] and $Ni_{40}Co_8Mn_{42}Sn_{10}$[15] alloys can reach up to 108.6 and 115 emu/g, respectively, showing a significant increase compared to ternary Ni-Mn-Sn alloys[16]. However, excessive Co doping may induce the formation of the γ second phase, which weakens the magnetization difference and increases thermal hysteresis, thereby diminishing the magnetocaloric effect[17]. According to literature reports[18,19], applying isostatic pressure can reduce the thermal hysteresis of NiMn-based alloys, and hydrostatic pressure will decrease the Mn-Mn atomic distance, reducing the unit cell volume. Additionally, researchers have achieved similar effects by introducing Si, a fifth element with a smaller atomic radius, to replace Sn, resulting in cell contraction. This approach aims to improve the thermal hysteresis of Co-doped alloys, synergistically regulating the magnetization difference and entropy change between phases, and optimizing the magnetocaloric effect of the alloys[20,21]. Therefore, it is essential to investigate the nature of changes in the physical properties of Ni-Mn-Sn alloys after Co doping and Co-Si co-doping by first-principles calculations.

Additionally, while element doping improves alloy properties, it also affects the martensite structure[14,22,23]. Martensite can be divided into modulated martensite and Non-modulated (NM) martensite. Modulated martensite includes four-layer orthorhombic (4O), five-layer modulated (5M), six-layer modulated (6M), and seven-layer modulated (7M) martensites. The twin boundary motion resistance of the NM martensite is significantly higher than that of modulated martensites. Therefore, it is more desirable for the alloy to undergo an intermediate modulated martensite transformation rather than directly transforming from austenite to NM martensite.

Researchers have found the existence of 6M martensite in Co-doped Ni-Mn-Sn alloys, but due to the complexity of the 6M structure, theoretical calculations on Ni-Co-Mn-Sn alloys is limited to austenite and NM martensite[4,14,15,24]. This led us to attempt to calculate the phase stability, magnetic properties, and electronic structure of 6M martensite in Ni-Co-Mn-Sn-(Si) alloy using first-principles calculations.

Based on the above research background, to achieve a more pronounced MCE, this study proposes balancing the roles of Co and Si through co-doping, building on the investigation of the physical properties of Co-doped $Ni_2Mn_{1.5}Sn_{0.5}$ alloys. This paper focuses on the effects of element

doping on the lattice changes, martensitic transformation, and magnetic properties in Ni-Mn-Sn-based alloys. Traditional experimental methods are time-consuming, labor-intensive, and costly. In contrast, first-principles calculations can not only determine the preferential occupancy of doped atoms, magnetic properties, and even possible martensitic transition sequences containing 6M martensite, but also guide experimental research and reveal the origin of related physical properties from the perspective of electronic structure.

2 Calculation details

The Vienna ab initio Simulation Package (VASP) based on the density functional theory (DFT) was used to perform the first-principles calculations, employing the projector augmented wave (PAW) pseudopotential approach to describe the interaction between ions and electrons[25-27]. The Perdew-Burke-Ernzerhof (PBE) implementation of generalized gradient approximation (GGA) was chosen to handle the exchange-correlation potential[28]. The valence electronic configurations of the relevant elements were Ni-$3d^8 4s^2$, Mn-$3d^6 4s^1$, Sn-$4d^{10} 5s^2 5p^2$, Co-$3d^8 4s^1$, and Si-$3s^2 3p^2$, respectively. The kinetic cutoff energy was set to 351 eV. The convergence criteria for total energy and atomic forces were established at 10^{-4} eV and 0.02 eV/Å, respectively.

As the experiments were conducted under low substituent concentrations, it is imperative to set constraints on the value of x and construct a 48-atom supercell to perform calculations for the austenite (Aus.), 6M and NM martensites at various doping concentrations. The structural relationship between the studied high-temperature austenite, the intermediate 6M martensite, and the low-temperature NM martensite is shown in Fig. 1. Depending on the initial lattice parameters, 10 × 4 × 10 k-point, 7 × 13 × 5 k-point, and 8 × 7 × 9 k-point were used for the austenite, 6M, and NM martensite, respectively. Detailed crystallographic data regarding 6M martensite can be found in Ref. 29.

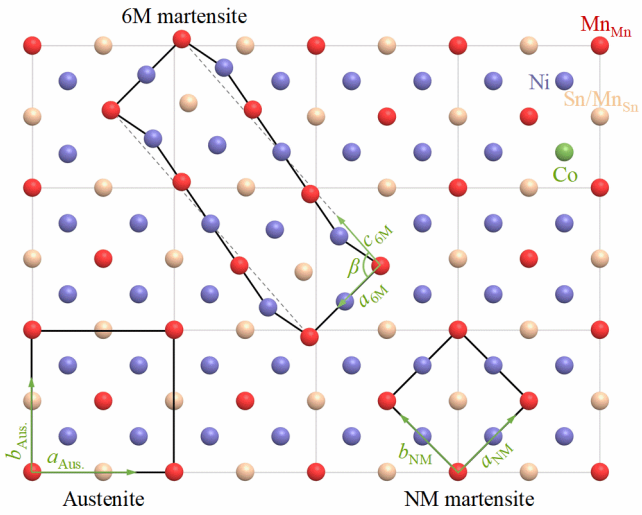

Fig. 1 Crystal structure of different phases of Ni-Mn-Sn-based alloys.

In prior studies, our research group established that additional Mn in the off-stoichiometric $Ni_2Mn_{1+x}Sn_{1-x}$ alloy exhibits a preference for occupying the Sn sublattice directly[30]. This led to the classification of Mn atoms into two distinct categories: Mn at the standard Mn site (Mn_{Mn}) and Mn occupying the Sn sublattice (Mn_{Sn}). Furthermore, all possible magnetic configurations were taken into account. Ferromagnetic (FM) and ferrimagnetic (FIM) signify the parallel and antiparallel alignment for the spin direction of Mn_{Mn} and Mn_{Sn} moments, respectively.

3 Results and discussion

3.1 Site preferences and magnetic configuration of Ni-Co-Mn-Sn alloys

The atomic occupation is one of the fundamental inquiries in exploring the physical properties related to the magneto-structural transition in Ni-Mn-based alloys. In investigating the physical properties of Ni-Co-Mn-Sn alloys, the primary task is to determine the preferred position of the fourth element Co in the alloy, as illustrated in Fig. 2. Due to the non-diffusive nature of martensitic transformation, once the optimal occupation of Co atoms in the austenite is determined, the corresponding 6M and NM martensitic structures are also established accordingly.

For individual Co doping (x = 0.08), we considered the "normal" occupancy where Co directly substitutes Ni, Mn_{Mn}, Mn_{Sn}, or Sn sublattice, denoted as Co→Ni, Co→Mn_{Mn}, Co→Mn_{Sn}, and Co→Sn, respectively. From Fig. 2, it is evident that the formation energies (E_{form}) for all normal occupancy are less than 0 meV/atom, and the E_{form} of normal occupation (Co→Ni) with FIM state is the lowest.

This indicates that the austenite containing Co is a thermodynamically stable state. Additionally, we considered the "abnormal" occupancy where Co substitutes Ni site, namely Co→Mn_{Mn}→Ni, Co→Mn_{Sn}→Ni, and Co→Sn→Ni, which means that Co atoms occupy Mn_{Mn}/Mn_{Sn}/Sn atoms, the occupied atoms move to the Ni sublattice. As seen from Fig.2, it is energetically optimal for Co to directly occupy the Ni sublattice (Co→Ni), since the E_{form} of the normal mode is much lowered than that of the abnormal modes.

Furthermore, to establish a more rational structural model, we also computed the dispersion degree of doped Co atoms in the $Ni_{1.83}Co_{0.17}Mn_{1.5}Sn_{0.5}$ alloy, including Co-Co cluster and disperse distributions. The E_{form} for the two occupancy configurations with the FM state are -74.79 and -74.23 meV/atom, respectively. The very small difference in E_{form} between these two distribution patterns suggests that the clustering or dispersion of Co atoms has a negligible effect on the E_{form} within this series of alloys. It is noteworthy that due to the slightly lower E_{form} associated with Co-Co clustering, we continued to utilize the Co-Co nearest-neighbor occupancy scheme in subsequent calculations. In summary, we ultimately opted for the atomic occupancy configurations that the doped Co atoms directly occupy Ni sites and Co-Co clustering distribution to design the austenite structures under different doping contents.

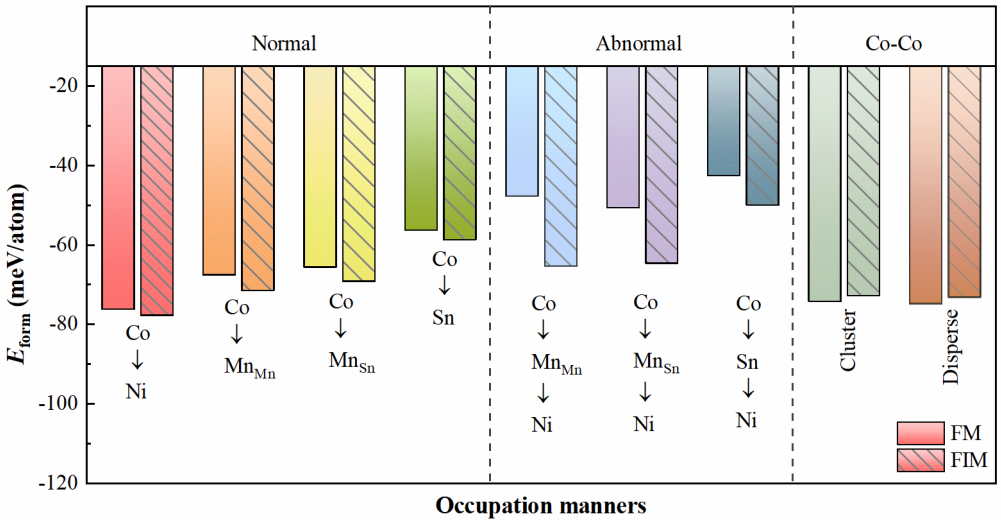

Fig. 2 Formation energy (E_{form}) dependence of occupation configuration of doped Co atoms for $Ni_{2-x}Co_xMn_{1.5}Sn_{0.5}$ (x = 0.08 and 0.17) alloys.

To determine the favorable magnetic states of each possible phase in the alloys at different doping contents, the dependence of E_{form} on Co content and magnetic configurations is illustrated in Fig. 3. As depicted, when x = 0 and 0.08, the E_{form} of three phases in the FIM state are lower than

those in the FM state. This indicates that each phase tends to adopt FIM configurations. With further increases in Co content, the E_{form} increment of the FIM austenite (FIA) becomes notably larger than that for the FM austenite (FA), rendering the FA more stable than the FIA in the composition range of $x \geq 0.17$. For the 6M martensite, the FIM state is maintained for $x \leq 0.33$, transitioning to the FM state at $x = 0.42$. Throughout the entire composition range considered, the FIM configuration remains energetically favorable for the NM martensite.

Therefore, it can be preliminarily concluded that with the gradual increase in Co content, the austenite transitions from the FIM state to the FM state at a lower Co content compared to the 6M martensite, while the NM martensite maintains the most stable FIM state. This indicates that substituting Ni with Co can effectively enhance the magnetization intensity of the austenite and 6M martensite, while the NM martensite remains weakly magnetic. This further confirms that Co doping stimulates the magnetic changes during the austenite to 6M or NM martensite structural transition in Ni-Co-Mn-Sn alloys, facilitating the attainment of a large magnetic moment difference (ΔM) during the martensitic transformation, thereby favoring significant magnetocaloric effects.

In addition, based on the scatter plot, we performed a linear fitting for the formation energies of different magnetic states of the phases as a function of Co content x, and obtained the corresponding fitting equations as shown in Eq (1)-(6).

(1) For the austenite:

$$E_{form\text{-}Aus.\text{-}FM}=19.69x-78.04 \quad (3\text{-}1)$$

$$E_{form\text{-}Aus.\text{-}FIM}=59.45x-82.85 \quad (3\text{-}2)$$

(2) For the 6M martensite:

$$E_{form\text{-}6M\text{-}FM}=17.33x-76.98 \quad (3\text{-}3)$$

$$E_{form\text{-}6M\text{-}FIM}=91.75x-102.07 \quad (3\text{-}4)$$

(3) For the NM martensite:

$$E_{form\text{-}NM\text{-}FM}=25.05x-84.75 \quad (3\text{-}5)$$

$$E_{form\text{-}NM\text{-}FIM}=83.78x-117.39 \quad (3\text{-}6)$$

Where $E_{form\text{-}Aus.\text{-}FM}$, $E_{form\text{-}Aus.\text{-}FIM}$, $E_{form\text{-}6M\text{-}FM}$, $E_{form\text{-}6M\text{-}FIM}$, $E_{form\text{-}NM\text{-}FM}$, and $E_{form\text{-}NM\text{-}FIM}$ are the formation energies of austenite, 6M and NM martensites in FM and FIM states, respectively, and x represents the Co content. These fitting equations facilitate the prediction of formation energies for various magnetic states at different Co doping contents. This predictive capability helps determine

the stable magnetic stats of each phase and assess the possibility of magneto-structural coupling transitions. Such approach simplifies alloy screening in experiments, providing a more straightforward and efficient method for alloy composition design and accelerating the development and application of materials.

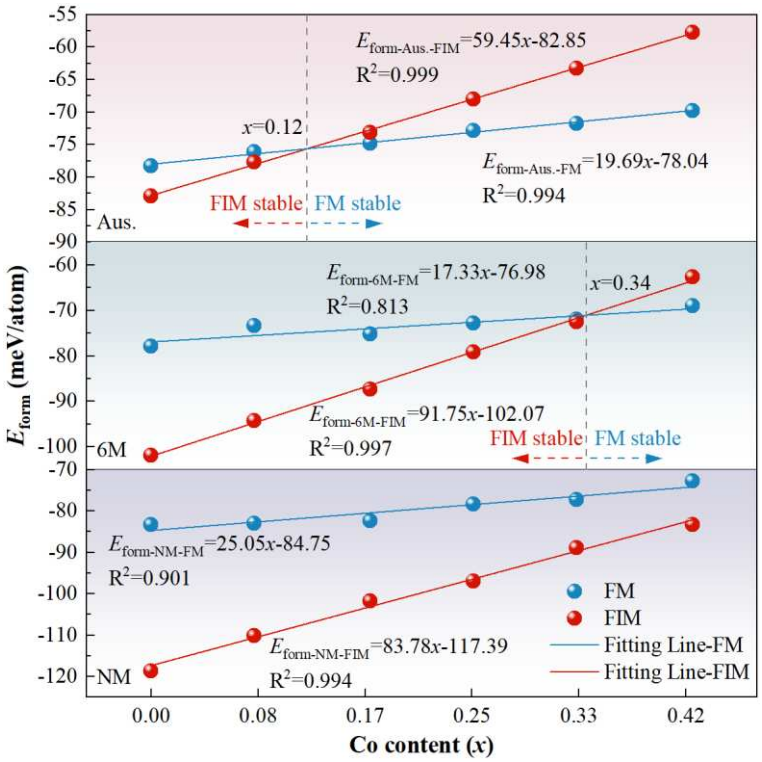

Fig. 3 Formation energy (E_{form}) of austenite, 6M and NM martensites for $Ni_{2-x}Co_xMn_{1.5}Sn_{0.5}$ (x = 0.00–0.42) alloys in different magnetic states.

3.2 Structural parameters of Ni-Co-Mn-Sn alloys

The structural parameters of $Ni_{2-x}Co_xMn_{1.5}Sn_{0.5}$ (x = 0–0.42) alloys, focusing on the equilibrium lattice constants of austenite, 6M and NM martensites in both FM and FIM states, are presented in Table 1. Regardless of the doping content and phase structure, it is noted that the crystal volume of the FM state consistently exceeds that of the FIM state. Similar phenomena have been reported in Ni-Mn-Ga[31] and Ni-Mn-In[32] alloys. Li *et al.*[31] attributed to magnetism where ferromagnetic phases tend to possess larger lattice constants compared to non-magnetic phase.

Table 1 Optimized lattice parameters and volume per formula unit of $Ni_{2-x}Co_xMn_{1.5}Sn_{0.5}$ (x = 0–0.42) alloys in FM and FIM states (Bold indicate optimal magnetic state of each phase).

Co content (x)	Aus.		6M					NM		
	a (Å)	V (Å^3)	a (Å)	b (Å)	c (Å)	β (°)	V (Å^3)	a (Å)	c (Å)	V (Å^3)

x = 0.00	FM	5.950	52.664	4.206	5.969	12.593	91.663	52.675	4.156	6.086	52.646
	FIM	**5.928**	**52.075**	**4.426**	**5.429**	**12.911**	**94.373**	**51.556**	**3.761**	**7.230**	**51.138**
x = 0.08	FM	5.947	52.573	4.314	5.705	12.825	92.886	52.541	4.182	6.005	52.516
	FIM	**5.926**	**52.017**	**4.409**	**5.449**	**12.900**	**94.293**	**51.505**	**3.764**	**7.191**	**50.948**
x = 0.17	FM	**5.944**	**52.491**	4.141	6.112	12.425	91.139	52.407	4.170	6.024	52.377
	FIM	5.923	51.936	**4.417**	**5.437**	**12.886**	**94.180**	**51.442**	**3.768**	**7.157**	**50.822**
x = 0.25	FM	**5.940**	**52.397**	4.174	6.061	12.435	90.728	52.419	4.196	5.936	52.268
	FIM	5.919	51.836	**4.398**	**5.458**	**12.874**	**94.059**	**51.373**	**3.776**	**7.125**	**50.798**
x = 0.33	FM	**5.938**	**52.343**	4.134	6.115	12.409	91.677	52.252	4.159	6.027	52.116
	FIM	5.916	51.754	**4.386**	**5.472**	**12.863**	**94.009**	**51.328**	**3.780**	**7.104**	**50.756**
x = 0.42	FM	**5.933**	**52.219**	**4.197**	**5.930**	**12.594**	**90.739**	**52.234**	4.193	5.933	52.161
	FIM	5.913	51.689	4.360	5.510	12.822	93.547	51.243	**3.789**	**7.069**	**50.739**

Regarding the optimal magnetic states and lattice constants of different phases at various doping content, it is observed that as the Co content increases from 0 to 0.17, the magnetic ground state of the austenite shifts from the FIM state to the FM state, resulting in an expansion of lattice constants and cell volume. However, with further increases in Co content, the lattice constant of the austenite in the FM state (a^{FM}) gradually decreases. Analysis reveals that the substitution of smaller Ni atoms (1.24 Å) by larger Co atoms (1.25 Å) causes a gradual reduction in lattice constants, indicating that this unique phenomenon cannot be solely explained by variations in atomic radii. Previous studies have indicated that factors influencing lattice constants include interatomic bonding strength and magnetism[33,34]. Hence, Fig. 4 illustrates the differential charge density in the plane containing Co atoms within the austenite structure, providing further insights into how these structural changes influence the magnetic and lattice properties of the alloys.

From the differential charge density plots depicted in Fig. 4(a_2) to (c_2), it is evident that larger Co atoms induce greater Ni-Co atomic distances compared to Ni-Ni distances. While, regardless of whether it is the FIA at x = 0.08 or the FA at x = 0.17 and x = 0.25, the Co-Mn distances are often shorter than the corresponding Ni-Mn distances. Correspondingly, in the two-dimensional plane of the differential charge density plot, it is observable that Co atoms, possessing larger atomic magnetic moments, exhibit stronger bonding with surrounding Mn atoms compared to Ni atoms. As the Co content increases from 0.17 to 0.25 (illustrated in Fig. 4(b_2) to (c_2)), the closest Co-Mn distances decrease further, elucidating the critical role of Co doping in reducing the a^{FM}. Furthermore, from Fig. 4(b_2) to (c_2), it is observed that the initially equal Mn_{Mn}-Mn_{Sn} distances become unequal. This is attributed to the introduction of the additional Co atom, which shortens the distance to its nearest

Mn_{Sn} neighbor, once again highlighting the stronger interaction between Co and Mn compared to Ni and Mn.

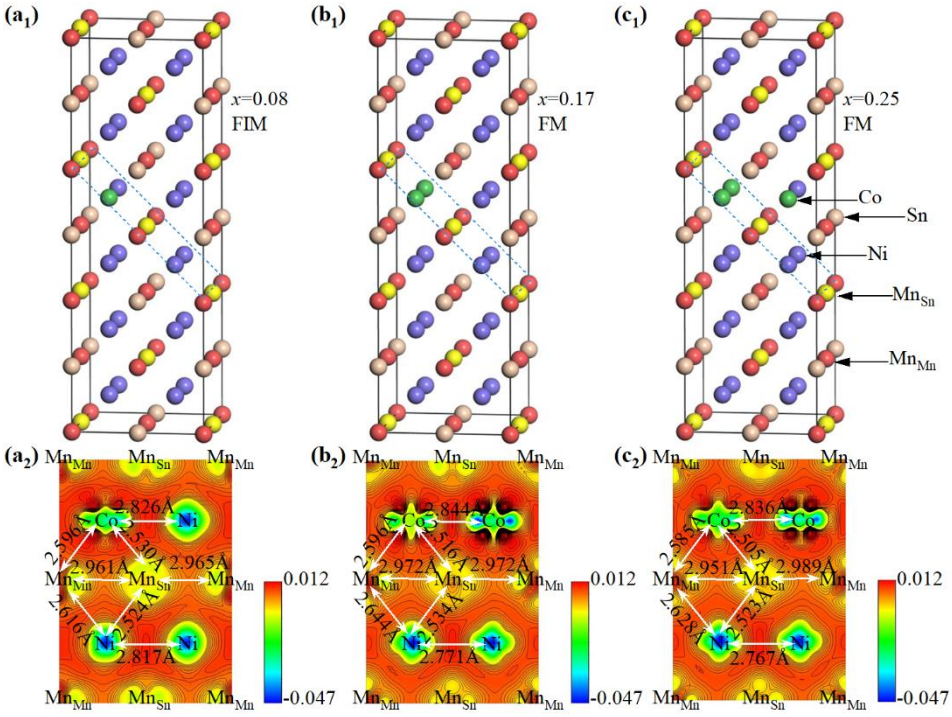

Fig. 4 Crystal structure of austenite and its differential charge densities on the plane with Co atoms for $Ni_{2-x}Co_xMn_{1.5}Sn_{0.5}$ (x = 0.08, 0.17, 0.25) alloys: (a_1)–(a_2) x = 0.08, (b_1)–(b_2) x = 0.17, and (c_1)–(c_3) x = 0.25.

Similarly, for the FIM configurations of 6M and NM martensites, the lattice volume gradually decreases progressively with increasing Co content. It is noteworthy to mention that slight volume contractions are evident during martensitic transformations (austenite→6M martensite→NM martensite (x = 0–0.33), austenite→NM martensite (x = 0.42)), which is consistent with the inherent characteristic of volume contraction during martensitic transformation.

3.3 Martensitic transformation of Ni-Co-Mn-Sn alloys

Based on the determination of the optimal magnetic states of different phases under various Co contents x in Section 3.1, Fig.5 illustrates the dependence of the formation energy of austenite, 6M and NM martensites in the $Ni_{2-x}Co_xMn_{1.5}Sn_{0.5}$ (x = 0–0.42) alloys. This assessment evaluates the influence of Co doping on phase stability and possible martensitic transformation sequence.

From Fig. 5(a), it is evident that the formation energies of various phases in the alloys gradually increase with the higher Co content. This trend is attributed to the differences in atomic radius and

electronegativity between the doping atom Co and the substituted atom Ni, which induce local lattice distortions and consequently reduce the stability of each phase. However, compared to the austenite, the rate of increase in formation energies for 6M and NM martensites is noticeably faster.

For $x < 0.33$, the sequence of phase stability is austenite, 6M martensite, and NM martensite based on the formation energies from high to low. According to thermodynamics of transformation, the alloy undergoes structural transformation from austenite to intermediate 6M martensite, and ultimately to NM martensite during cooling. However, when $x = 0.33$, the formation energies of 6M martensite in both FM and FIM states are very close to the formation energy of FM austenite. The more stable FIM state of 6M martensite has a formation energy of only 0.83 meV/atom lower than that of FM austenite, indicating a very small driving force for the transformation from austenite to 6M martensite, suggesting difficulty in this phase transformation. Nevertheless, the E_{form} of NM martensite is significantly lower than that of austenite, allowing for a one-step martensite transformation from austenite to NM martensite. At x=0.42, the E_{form} of 6M martensite is higher than that of austenite, indicating lower stability of 6M martensite compared to austenite, so the alloy can only undergo one-step martensitic transformation.

Taking into account the optimal magnetic configurations of each phase, the possible martensitic transformation sequences in the $Ni_{2-x}Co_xMn_{1.5}Sn_{0.5}$ alloys during cooling are outlined as follows: $Aus.^{FIM} \rightarrow 6M^{FIM} \rightarrow NM^{FIM}$ ($0 \leq x < 0.08$), $Aus.^{FIM/FM} \rightarrow 6M^{FIM} \rightarrow NM^{FIM}$ ($0.08 \leq x < 0.25$), $Aus.^{FM} \rightarrow 6M^{FIM} \rightarrow NM^{FIM}$ ($0.25 \leq x < 0.33$), $Aus.^{FM} \rightarrow NM^{FIM}$ ($0.33 \leq x \leq 0.42$).

It is worth noting that in the subsequent discussion, when a phase can coexist in two magnetic states, the magnetic state with relatively lower formation energy is chosen for analysis and discussion for convenience.

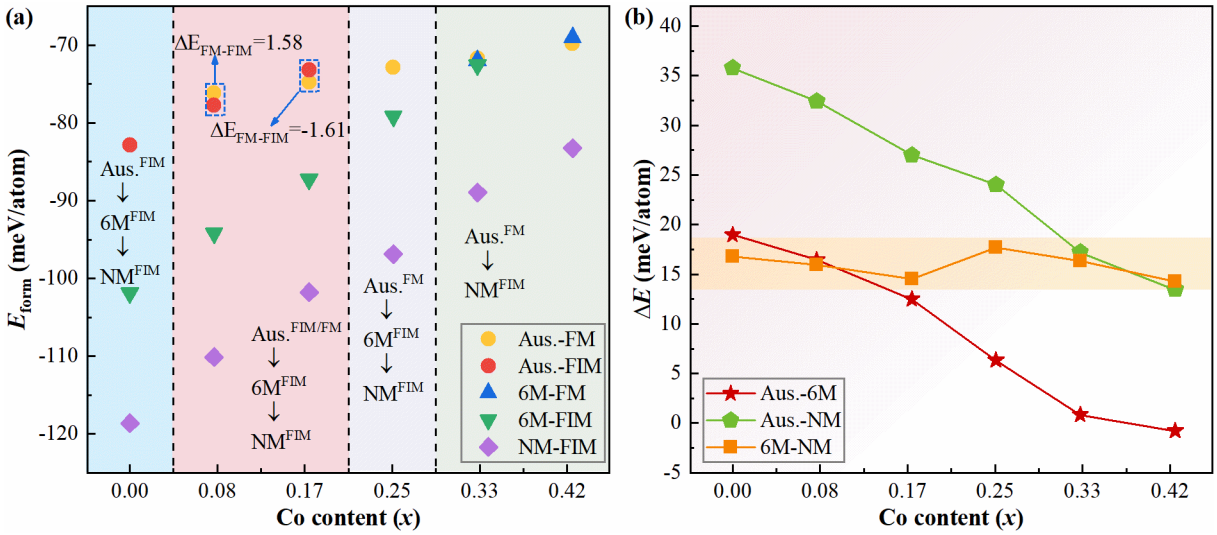

Fig. 5 (a) Formation energies (E_{form}) of each phase and (b) energy differences ΔE between phases of $Ni_{2-x}Co_xMn_{1.5}Sn_{0.5}$ (x = 0.08–0.42) alloys.

Meanwhile, the energy differences between each phase under various compositions are calculated to investigate the possibility of phase transformation and elucidate the intrinsic mechanism of transformation temperature (T_M) variation with Co content, as shown in Fig. 5(b). Both theoretical and experimental evidence indicate that the energy difference is approximately proportional to the martensitic transformation temperature[35,36]. A larger energy difference indicates a greater driving force for the alloy to transform from austenite to 6M or NM martensites, facilitating martensitic transformation and resulting in higher T_M.

From the graph, it is evident that with increasing Co content, the energy differences ($\Delta E_{Aus.-6M}$ and $\Delta E_{Aus.-NM}$) between austenite and 6M/NM martensite show a linear decreasing trend. This suggests that T_M gradually decreases with increasing Co content, consistent with experimental observations where Co doping lowers the phase transition temperature. As for the energy difference between 6M and NM martensites (ΔE_{6M-NM}), it only exhibits slight fluctuations within a certain energy range, indicating a minor dependence on Co content at lower Co doping content, suggesting that Co doping has minimal impact on the transformation temperature of intermediate martensite transformation.

The possible martensitic transformation sequence of this alloy system, considering other factors influencing T_M, is summarized in Table 2. In addition to analyzing T_M based on phase transition driving forces, parameters such as valence electron concentration (e/a), electron density (n)

$n=\frac{(e/a)\times N}{V_{cell}}$ [37], and martensite tetragonal distortion ($|c/a-1|$)[38,39](the lattice constants a and c of the basic martensitic crystal structure are based in the parent phase coordinate) provide effective predictive capabilities for T_M. As shown in the table, these parameters decrease gradually with increasing Co content, predicting a reduction in T_M, which aligns with results obtained from the analysis of phase transition driving forces.

Table 2 Possible martensitic transformation sequence, valence electron concentration (e/a), density of electrons (n), and tetragonality of martensite ($|c/a-1|$) for $Ni_{2-x}Co_xMn_{1.5}Sn_{0.5}$ (x = 0–0.42) alloys.

Co content	Possible martensitic transformation sequences	e/a	n	$\|c/a-1\|$
x = 0.00	$Aus.^{FIM}\rightarrow 6M^{FIM}\rightarrow NM^{FIM}$	8.125	0.6241	0.359
x = 0.08	$Aus.^{FIM/FM}\rightarrow 6M^{FIM}\rightarrow NM^{FIM}$	8.104	0.6232	0.351
x = 0.17	$Aus.^{FIM/FM}\rightarrow 6M^{FIM}\rightarrow NM^{FIM}$	8.083	0.6160	0.343
x = 0.25	$Aus.^{FM}\rightarrow 6M^{FIM}\rightarrow NM^{FIM}$	8.063	0.6155	0.334
x = 0.33	$Aus.^{FM}\rightarrow NM^{FIM}$	8.042	0.6146	0.329
x = 0.42	$Aus.^{FM}\rightarrow NM^{FIM}$	8.021	0.6144	0.319

To further explore the origin of the martensitic transformation in the $Ni_{2-x}Co_xMn_{1.5}Sn_{0.5}$ alloys from an electronic structure perspective, the total density of states (DOS) of austenite, 6M and NM martensites were calculated, as depicted in Fig. 6. It is well-established that phase stability is closely linked to the presence of spin-down states near the Fermi level (E_F). From Fig. 6, notable peaks appear near the E_F can be observed for the austenites across all studied alloy compositions. This observation suggests that a potential instability of the austenite could lead to further phase transitions, consistent with the formation energy results. During the martensitic transformation, the E_F shifts from the peak of austenite towards the pseudo-gap in the 6M and NM martensites, i.e., the band Jahn-Teller effect[40]. In $Ni_{1.58}Co_{0.42}Mn_{1.5}Sn_{0.5}$ alloy, the similarity in DOS between austenite and 6M martensite results in an insufficient driving force for the transformation from austenite to 6M martensite. This likely explains the absence of an intermediate martensitic transformation in this alloy. (您的提问“能不能加这个成分发生相变的参考文献”—转换到实验成分便是 $Ni_{39.5}Co_{10.5}Mn_{37.5}Sn_{12.5}$,因为有析出相导致马氏体相变消失，这部分我做过实验，所以也就没放实验，参考文献中与这个成分相似的也是不能发生马氏体相变)

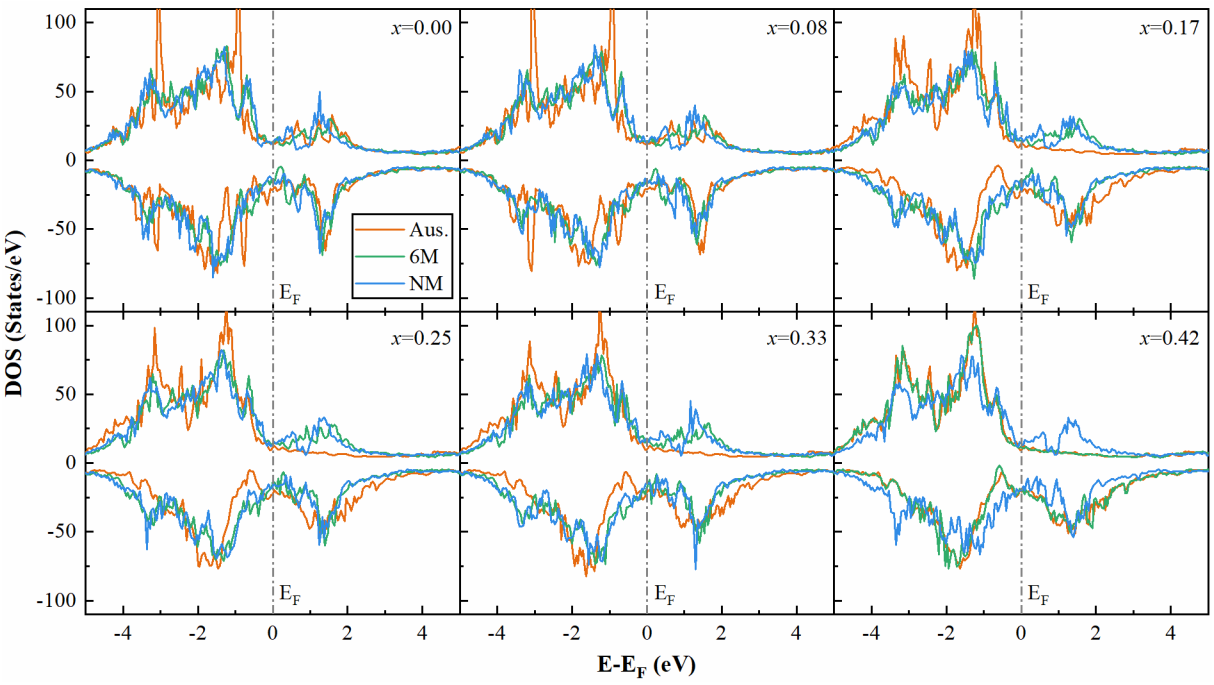

Fig. 6 Total density of states (DOS) of austenite, 6M and NM martensites for $Ni_{2-x}Co_xMn_{1.5}Sn_{0.5}$ alloys. Zero energy is regarded as E_F.

3.4 Magnetic properties of Ni-Co-Mn-Sn alloys

Fig. 7 illustrates the total magnetic moments of austenite, 6M and NM martensites with stable magnetic configurations in the $Ni_{2-x}Co_xMn_{1.5}Sn_{0.5}$ ($x = 0$–0.42) alloys. As Co atoms, which have larger magnetic moments, substitute Ni atoms with smaller magnetic moments, there is a gradual increase in the total magnetic moments of each phase overall. A larger ΔM can facilitate the generation of greater magnetic driving forces during phase transitions. However, in the Mn-rich Sn-deficient $Ni_2Mn_{1+x}Sn_{1-x}$ alloys, there exists an antiferromagnetic interaction between Mn_{Mn} and Mn_{Sn} atoms. Therefore, for $x \leq 0.08$, only a small ΔM can be observed between the austenite and martensite phases, which is unfavorable for the magnetic-field-induced reverse martensitic transformation. It is not until the Co content reaches 0.17 that a magneto-structural coupling transition occurs from FM austenite to FIM martensite, resulting in a larger ΔM during the phase transformation. A larger ΔM makes the alloy a potential candidate for magnetic shape memory materials, thereby providing possibility of martensitic transformation and mechanical actuation induced by a strong magnetic field. This elucidates the rationale behind researchers utilizing Co alloying to tailor the magnetic properties of Ni-Mn-based alloys.

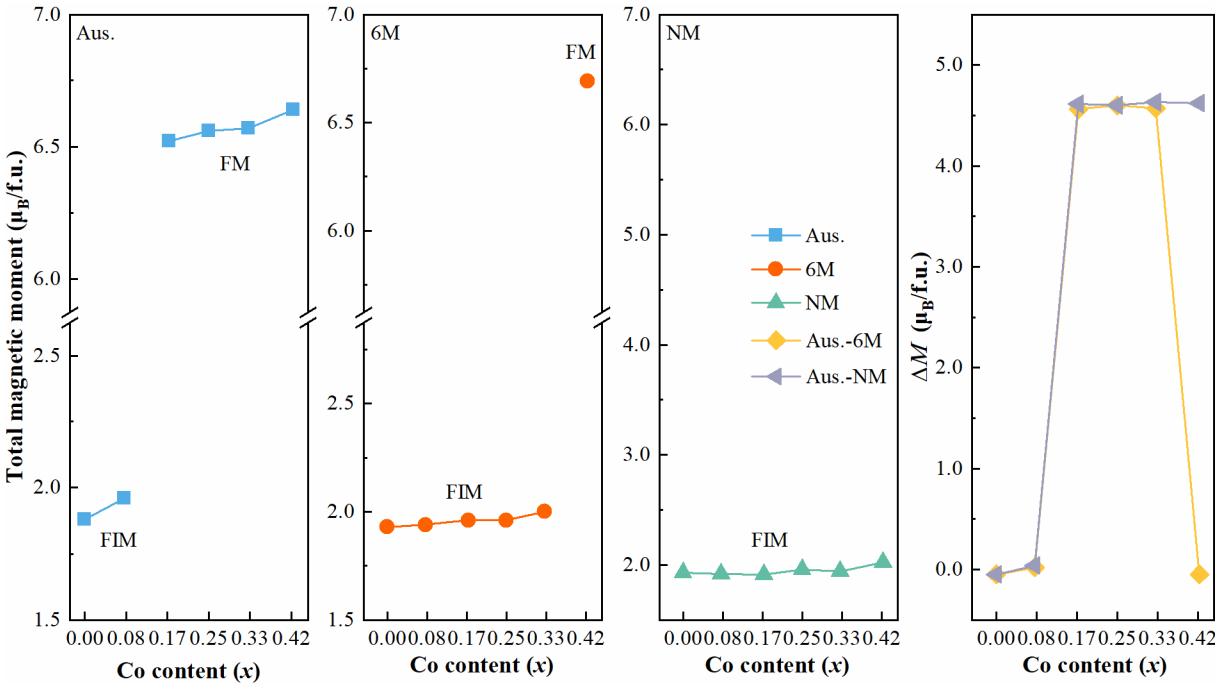

Fig. 7 Total magnetic moment per formula unit in austenite, 6M and NM martensites as well as $\triangle M$ of Aus.-6M and Aus.-NM for $Ni_{2-x}Co_xMn_{1.5}Sn_{0.5}$ alloys.

Furthermore, to explore deeper into the reasons behind variations in the total magnetic moments of each phase with composition, this section also calculates the atomic magnetic moments of Ni, Mn, and Co atoms in the austenite, 6M and NM martensites, as depicted in Fig. 8. It should be noted that the magnetic moments of different types of atoms in the alloy exhibit a range of values. Therefore, to clearly demonstrate the trends in atomic magnetic moments with composition, "I" symbols represent the range of atomic magnetic moments, while the average values of each type of atomic moment were calculated and denoted by dots. The contribution of Sn moments (-0.099–-0.058 μ_B/atom) to the total magnetic moment is negligible.

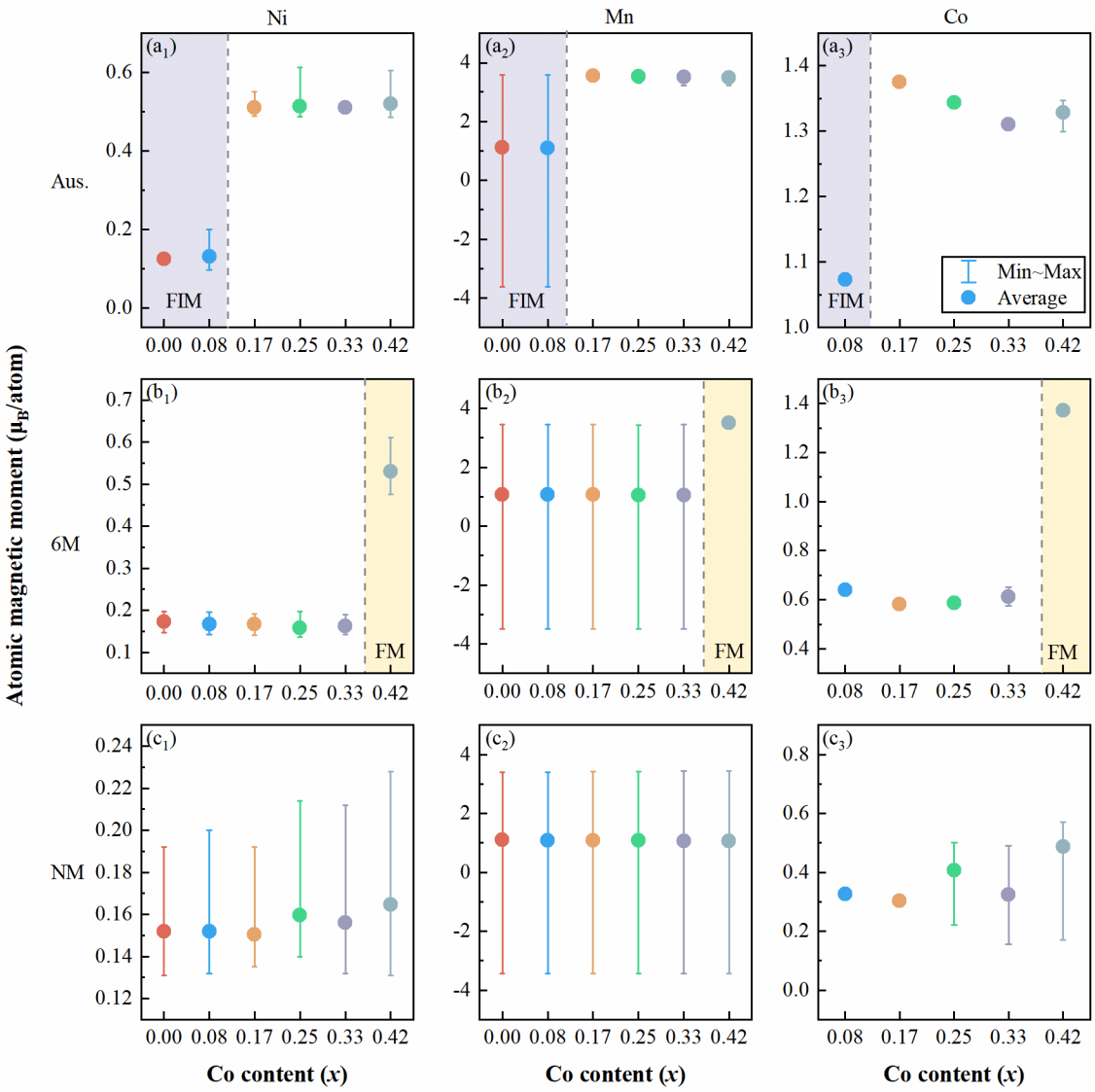

Fig. 8 Atomic magnetic moment of (a_1)–(a_3) austenite, (b_1)–(b_3) 6M martensite, and (c_1)–(c_3) NM martensite for $Ni_{2-x}Co_xMn_{1.5}Sn_{0.5}$ (x = 0–0.42) alloys.

It is evident from Fig. 8 that the magnetic moment of Mn atoms predominantly contributes to the total magnetic moment of each phase. In austenite, the magnetic moments of Ni, Mn, and Co show significant increases as Co content increases from 0.08 to 0.17, thereafter remaining relatively stable, as shown in Fig. 8(a_1)–(a_3). This trend arises because, at x = 0.08, Mn atoms with negative moments counterbalance the total magnetic moment of the austenite, resulting in a relatively weak ferromagnetic environment within the austenitic structure. This observation also corroborates the existence of Mn-Mn antiparallel arrangements in the FIM configuration. When $x \geq 0.17$, the magnetic moments of Mn atoms in the austenite become positive (approximately 3.45 μ_B/atom) (Fig. 8(a_2)), leading to a ferromagnetic state in austenite.

Similarly, in 6M martensite, the presence of antiparallel arrangement of Mn directly influences the magnitude of the Ni and Co moments (Fig. 8(b_1)–(b_3)). In the case of NM martensite, although there are slight fluctuations in the Ni and Co moments, overall they increase with higher Co content, roughly corresponding to the trend observed in the total magnetic moment.

For the $Ni_{2-x}Co_xMn_{1.5}Sn_{0.5}$ (x = 0–0.42) alloys, the nearest-neighbor atomic distances of each phase have also been calculated and shown in Fig. 9. The data reveal that the Co-Mn atomic distances are generally smaller than Ni-Mn distances in all phases, indicating a stronger bonding between Co-Mn compared to Ni-Mn, which aligns with the findings drawn in Section 3.2. Furthermore, by comparing the Mn-Mn distances across different phases at the same composition, it is evident that the variations in these distances lead to an antiparallel arrangement of Mn_{Mn} and Mn_{Sn} moments. This configuration significantly reduces the ferromagnetic environment around Mn atoms, facilitating the formation of a martensite ferrimagnetic environment. This phenomenon can be explained through both direct interactions (the Bethe-Slater curve) and indirect exchange interactions via conduction electrons (RKKY interaction)[41]. As Mn_{Mn}-Mn_{Sn} atomic distance decreases to a critical value, demagnetization effects may cause a reversal in the spin direction of Mn_{Sn} moment, establishing a magnetic equilibrium state. This underpins the magneto-structural coupling transformation observed in the $Ni_{2-x}Co_xMn_{1.5}Sn_{0.5}$ (x = 0.17–0.42) alloys. Notably, in the x = 0.42 alloy, the Mn-Mn atomic distance in 6M martensite increases sharply, exceeding that in austenite, indicating parallel alignment of all Mn moments. This elucidates the stability of 6M martensite in the FM state for this composition.

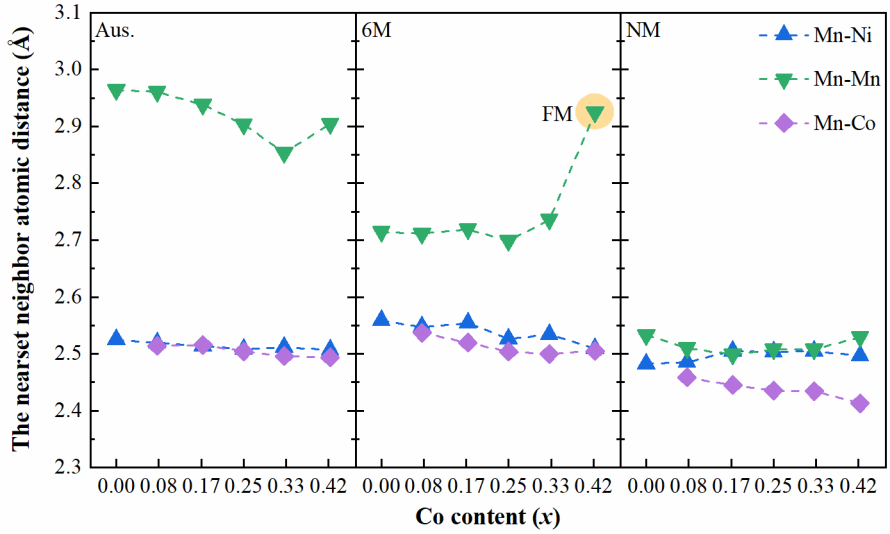

Fig. 9 The nearest neighbor atomic distance of austenite, 6M and NM martensites for $Ni_{2-x}Co_xMn_{1.5}Sn_{0.5}$ (x = 0–0.42) alloys.

3.5 Physical characteristics of Si-doped Ni-Co-Mn-Sn alloys

Based on the investigation mentioned above into the relevant physical properties of Ni-Co-Mn-Sn alloy, this section focuses on a theoretical exploration of Si doping in the $Ni_{1.75}Co_{0.25}Mn_{1.5}Sn_{0.5}$ alloy, supercell containing 48 atoms to conduct a small quantity of Si doping to clarify Si introduction on the phase stability, magnetism and thermal hysteresis of the alloy. The $Ni_{1.75}Co_{0.25}Mn_{1.5}Sn_{0.5}$ alloy was chosen as the base alloy due to its large $\triangle M$, although doped Co increases phase transformation hysteresis. Substituting smaller-radius Si contracts the unit cell, reducing hysteresis and enhancing the alloy's reversible magnetocaloric effect.

First, the preferential occupation of Si in the $Ni_{1.75}Co_{0.25}Mn_{1.5}Sn_{0.5}$ alloy was explored from a thermodynamic perspective. Five possible configurations were considered: doped Si atom directly occupies the sublattices of Ni, Mn_{Mn}, Mn_{Sn}, Sn, or Co, denoted as Si→Ni, Si→Mn_{Mn}, Si→Mn_{Sn}, Si→Sn, and Si→Co, respectively. The detailed atomic occupation information is depicted in the schematic crystal structure illustrated in Fig. 10. Additionally, Fig. 10 showcases the formation energies and total magnetic moments corresponding to different magnetic states of the austenite when Si occupies distinct sites.

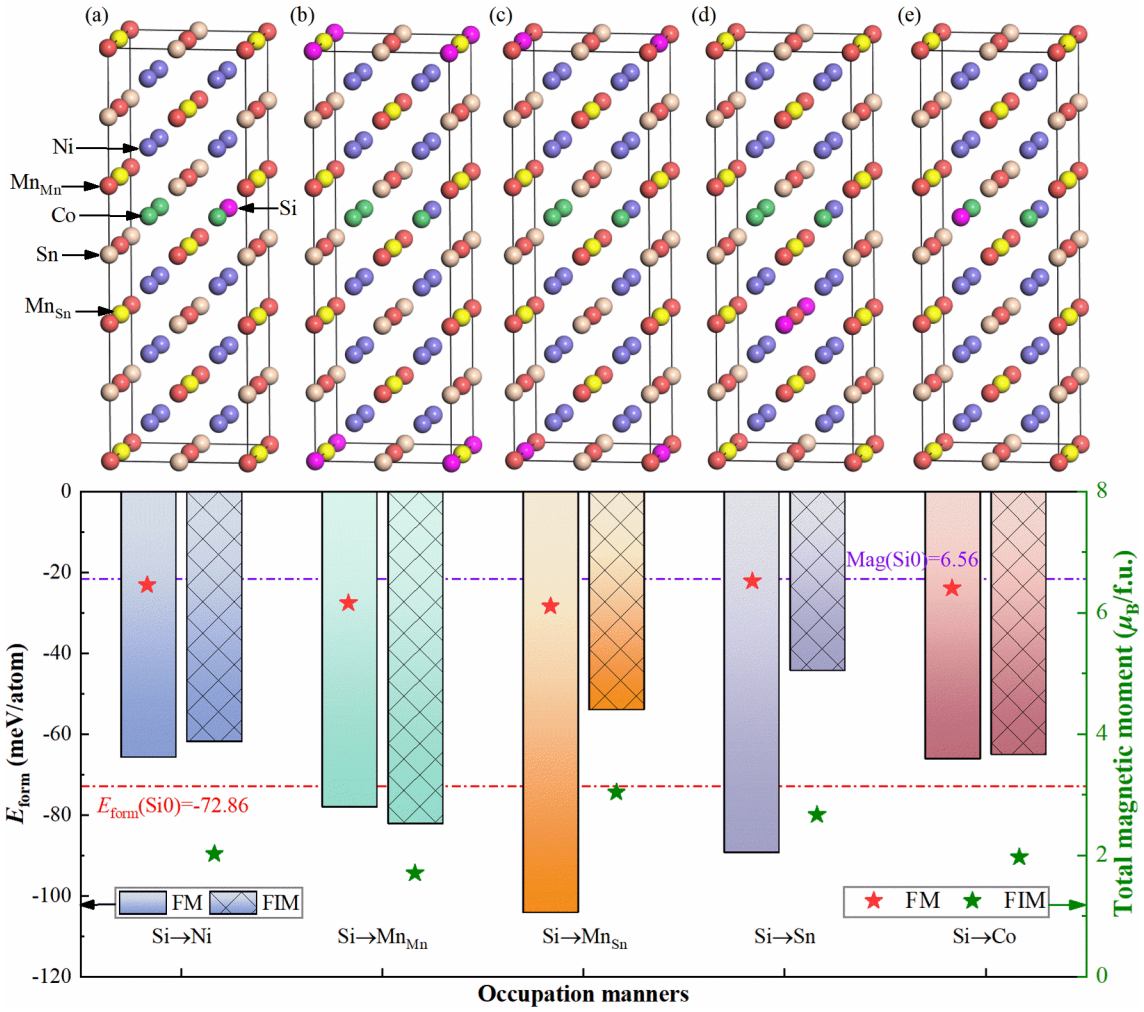

Fig. 10 Crystal structure, formation energies, and total magnetic moments of Si substitution in austenite for (a) $Ni_{1.67}Si_{0.08}Co_{0.25}Mn_{1.5}Sn_{0.5}$, (b) and (c) $Ni_{1.75}Co_{0.25}Mn_{1.42}Si_{0.08}Sn_{0.5}$, (d) $Ni_{1.75}Co_{0.25}Mn_{1.5}Sn_{0.42}Si_{0.08}$, and (e) $Ni_{1.75}Co_{0.17}Si_{0.08}Mn_{1.5}Sn_{0.5}$ alloys.

The red and purple dot-dash lines in Fig. 10 respectively represent the formation energy and total magnetic moment of the FM austenite in the $Ni_{1.75}Co_{0.25}Mn_{1.5}Sn_{0.5}$ alloy without Si doping (denoted as Si0). It is evident from Fig.10 that the E_{form} of the FM austenite increases relative to the Si0 alloy when Si replaces Ni or Co, indicating a decrease in the stability of the austenite. Conversely, when Si substitutes Mn (Mn_{Mn} and Mn_{Sn}) or Sn site, the E_{form} of the FM austenite decreases, suggesting an increase in phase stability. Thermodynamically, the FIM austenitic is the most stable when Si directly replaces Mn_{Sn} site among these five substitution configurations. Simultaneously, the total magnetic moment of the austenite varies with the different Si occupations, as indicated by the pentagram symbols in Fig. 10. When the non-magnetic element Si substitutes for the paramagnetic Sn or for Ni and Co atoms with small atomic magnetic moments, the total magnetic moment decreases

slightly. (可不可以改成：When Si substitutes for Ni, Sn, or Co, the total magnetic moment decreases slightly.&&&可以)However, a more significant change in the total magnetic moment is observed when Si replaces the ferromagnetic Mn atom.

Based on the determination of the optimal substitution site of Mn_{Sn} by Si, the E_{form} of the 6M and NM martensites in the $Ni_{1.75}Co_{0.25}Mn_{1.42}Si_{0.08}Sn_{0.5}$ alloy (Si0.08) under FM and FIM states were calculated, as shown in Fig. 11(a). Additionally, Fig. 11(b) presents the formation energies and total magnetic moments of both the undoped alloy (Si0) and the Si-doped alloy (Si0.08) in FM and FIM states. It is evident that the Si doping reduces the formation energy of each phase in the $Ni_{1.75}Co_{0.25}Mn_{1.5}Sn_{0.5}$ alloy, thereby enhancing the phase stability. Furthermore, the formation energies of stable magnetic states for austenite, 6M and NM martensites in the Si0.08 alloy decrease sequentially, indicating that this alloy can undergo a magneto-structural coupled phase transition of $Aus.^{FM}\rightarrow 6M^{FIM}\rightarrow NM^{FIM}$. Additionally, Si doping reduces both $\Delta E_{Aus.-NM}$ and $\Delta E_{Aus.-6M}$, indicating a decrease in the driving force for the martensitic transformation. This suggests that the martensitic transformation temperature decreases with Si doping.

To investigate the physical mechanism of phase stability, the DOS of the austenite, 6M and NM martensites of the $Ni_{1.75}Co_{0.25}Mn_{1.42}Si_{0.08}Sn_{0.5}$ alloy were calculated from an electronic structure perspective, as shown in Fig. 12(a). The spin-down DOS of austenite is not only stronger at the Fermi level compared to 6M and NM martensites, but it also exhibits a significant peak around -0.3 eV. This indicates that the instability of the austenite leads to further transformation, consistent with the formation energy results.

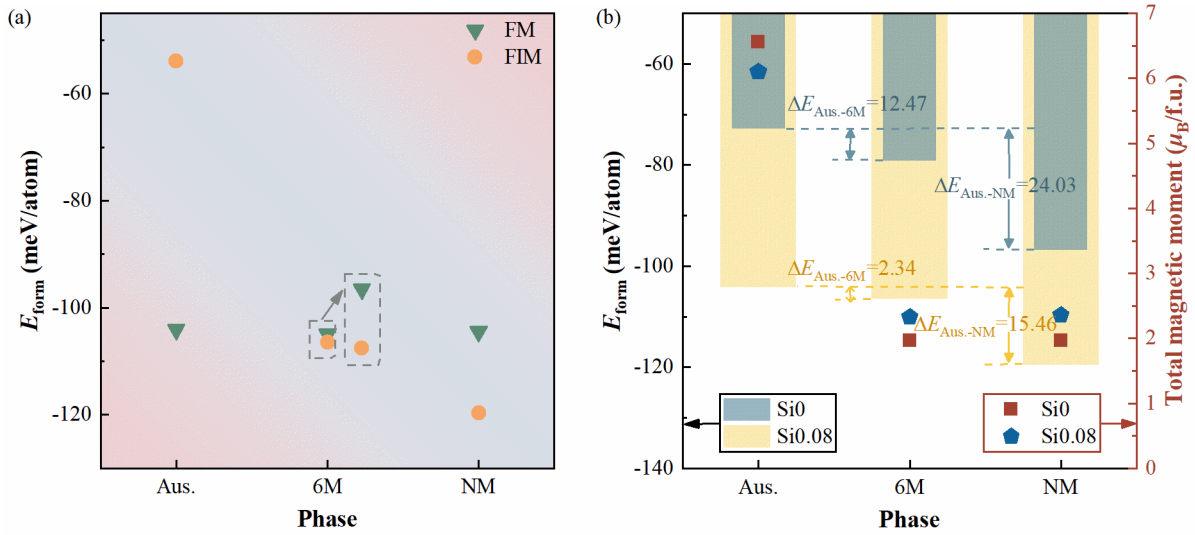

Fig. 11 (a) E_{form} of austenite, 6M and NM martensites for $Ni_{1.75}Co_{0.25}Mn_{1.42}Si_{0.08}Sn_{0.5}$ alloy (Si0.08) in FM and FIM states, (b) E_{form} and total magnetic moment of austenite, 6M and NM martensites for $Ni_{1.75}Co_{0.25}Mn_{1.5}Sn_{0.5}$ (Si0) and $Ni_{1.75}Co_{0.25}Mn_{1.42}Si_{0.08}Sn_{0.5}$ alloys (Si0.08) in stable magnetic state.

From Fig. 11(b), it can be observed that the total magnetic moment of the Si0 and Si0.08 alloys shows a slight decrease when Si substitutes Mn_{Sn} site in the FM austenite. This reduction is because the magnetic moment of the Si (-0.053 μ_B/atom) is much smaller than that of the Mn_{Sn} (3.469–3.635 μ_B/atom). Additionally, the total magnetic moment of the alloy is determined by the difference in the number of spin-up and spin-down electrons below the Fermi level ($\triangle N$). For the Si0 and Si0.08 alloys, the $\triangle N$ is 74.227 and 70.199, respectively. The decrease in $\triangle N$ leads to a reduction in the total magnetic moment, which fundamentally explains the changes in the magnetic properties of the austenite.

In contrast, the total magnetic moment of the FIM 6M and FIM NM martensites increases slightly because the paramagnetic Si atom has a larger moment than the Mn_{Sn} atom (-3.533–-3.273 μ_B/atom). Comparing Figs. 12(b)-(d), the DOS for spin-up and spin-down electrons below the Fermi level in austenite (Fig.12(b)) shows poorer symmetry compared to the 6M and NM martensites in Figs. 12(c) and 12(d), respectively. This indicates that the austenite possesses higher magnetism compared to the 6M and NM martensites. Although the magnetization difference during the phase transition is slightly reduced in the Si0.08 alloy compared to the Si0 alloy, it still maintains a significant magnetization difference during the cooling process ($\Delta M_{Aus.-6M}$.=3.78 μ_B/f.u. and $\Delta M_{Aus.-NM}$.=3.75 μ_B/f.u.).

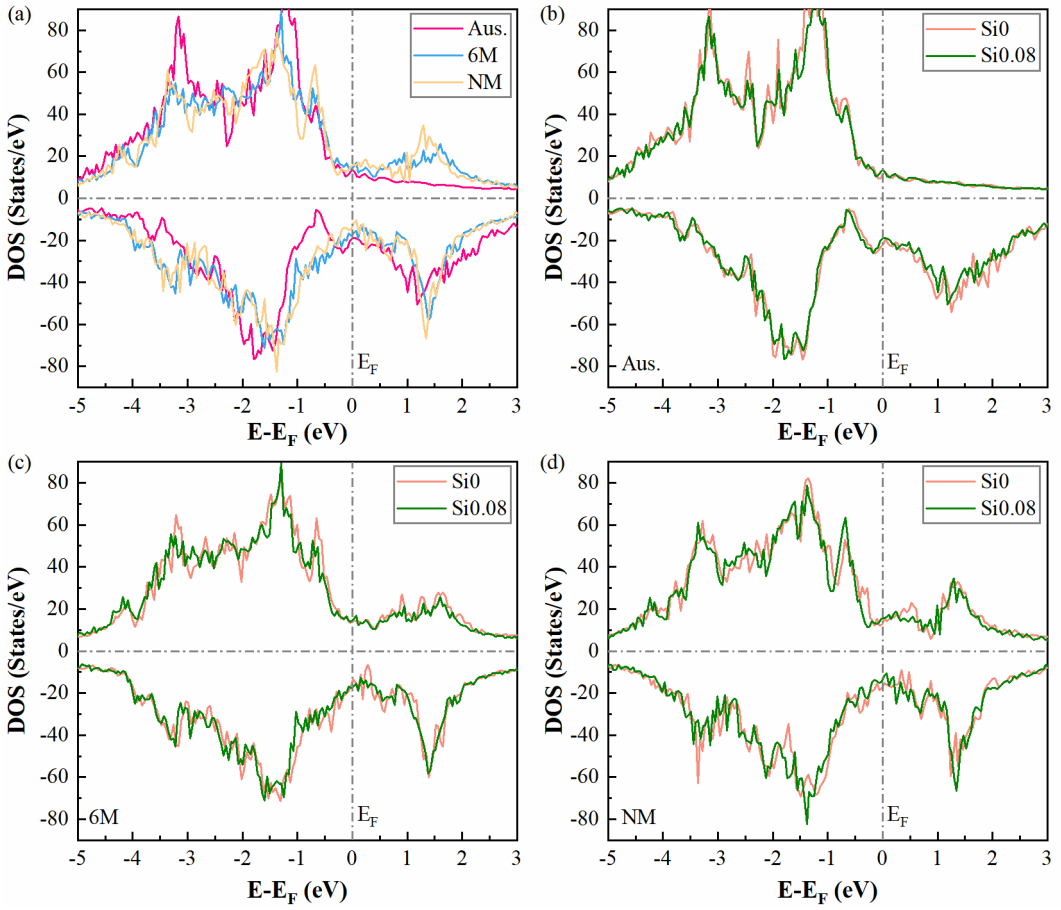

Fig. 12 Total density of states (DOS) of (a) austenite, 6M and NM martensites for Si0.08 alloy, (b) austenite, (c) 6M martensite, (d) NM martensite for Si0 alloy.

Moreover, according to the martensitic geometrically nonlinear theory applicable to all structural transformations as proposed by Cui et al.[42], the hysteresis behavior is closely related to crystal symmetry and the geometric compatibility between different phases. Typically, the hysteresis phenomenon can be qualitatively described by the tetragonal distortion strain $\varepsilon = (c/a)^{2/3}-1$ or the volume change $\Delta V_{\text{Aus-NM}}$ during the phase transition (the lattice distortion originates from frictional resistance during the phase transition, which to some extent leads to hysteresis)[43,44]. A smaller ε and $\Delta V_{\text{Aus-NM}}$, indicates reduced thermal hysteresis. To elucidate the intrinsic effects of Si doping on the phase transition hysteresis, we calculated the relevant lattice parameters for the FM austenite, FIM 6M martensite, and FIM NM martensite structures in the Si0.08 alloy and compared them with the undoped Si0 alloy. The results are summarized in Table 2.

Table 2 Lattice parameters related to crystal structure of $Ni_{1.75}Co_{0.25}Mn_{1.5-x}Si_xSn_{0.5}$ (x = 0, 0.08) alloys.

Alloys	Phases	a/Å	b/Å	c/Å	β/°	c/a	Volume/Å^3	$\Delta V_{\text{Aus-NM}}$/Å^3
Si0	Aus.	5.940	5.940	5.940	90	--	52.397	--
	6M	4.398	5.458	12.874	94.059	--	51.373	--

	NM	3.776	3.776	7.125	90	1.334	50.798	1.599
	Aus.	5.928	5.928	5.928	90	--	52.082	--
Si0.08	6M	4.356	5.517	12.816	94.454	--	51.169	--
	NM	3.816	3.816	7.003	90	1.298	50.979	1.103

As shown in Table 2, substituting Mn_{Sn} with Si leads to a reduction in the unit cell volume of austenite, 6M and NM martensites. This reduction is attributed to the significant atomic radius difference between Si (1.17 Å) and Mn (1.32 Å). The introduction of Si in small amounts causes a decrease in the *c*/*a* ratio (The lattice constants *a* and *c* of the basic martensitic crystal structure are based in the parent phase coordinate) of NM martensite, which in turn reduces the tetragonal distortion strain ε. During structural transition, both alloys exhibit volume contraction, but the Si-doped alloy shows a smaller volume change compared to the undoped alloy. The reduced lattice distortion indicates lower frictional resistance during phase transition. Based on these lattice parameters change, it is predicted that doping a small amount of Si can effectively reduce phase transformation hysteresis in the alloy. The thermal hysteresis of $Ni_{48}Mn_{39.5}Sn_{12.5-x}Si_x$ (x = 0，1，2) alloys decreased with increasing Si content (21.5 K → 16 K → 15 K)[21]. Similarly, Yang et al.[45] observed in experiments that the thermal hysteresis of $Ni_{39}Co_9Mn_{42}Sn_{10-x}Si_x$ (x = 0，1，2) alloys significantly decreased as Si content increased (35.2 K → 14.2 K → 6.6 K). Although current experiments primarily focus on reducing thermal hysteresis during phase transitions by substituting Sn with Si, our first-principles calculation results indicate that substituting Mn_{Sn} sublattice with Si can also reduce thermal hysteresis. This finding provides theoretical support for further alloy design.(这段保留是想说明通过理论计算发现不只是 Si 替代 Sn 可以降低之后，这位实验探索提供了另一种思路)可以保留，算讨论的部分

4 Conclusions

In summary, by first-principles calculations, the martensitic transformation sequence, magnetic properties, and electronic structure of $Ni_{2-x}Co_xMn_{1.5}Sn_{0.5}$ (x = 0–0.42) alloys were investigated systematically. The doped Co atoms tend to occupy the Ni sublattice directly, and the dispersion degree of doped Co has minimal impact on the alloy's phase stability. The volumes of FA, 6M ^{FIM} and NM ^{FIM} martensites gradually decrease with increasing Co content, due to the stronger bonding of Co with surrounding atoms. The possible martensitic transformation sequences in the $Ni_{2-x}Co_xMn_{1.5}Sn_{0.5}$ alloys during cooling are as follows: $Aus.^{FIM} \rightarrow 6M^{FIM} \rightarrow NM^{FIM}$ ($0 \leq x < 0.08$),

Aus.$^{FIM/FM}$→6M^{FIM}→NM^{FIM} ($0.08 \leq x < 0.25$), Aus.^{FM}→6M^{FIM}→NM^{FIM} ($0.25 \leq x < 0.33$), Aus.^{FM}→NM^{FIM} ($0.33 \leq x \leq 0.42$). Subsequently, the $Ni_{1.75}Co_{0.25}Mn_{1.5}Sn_{0.5}$ alloy with potential for excellent magnetic properties was selected for alloying with a small amount of Si doping. The preferential occupation of Si atoms in the Mn_{Sn} sublattice of the $Ni_{1.75}Co_{0.25}Mn_{1.5}Sn_{0.5}$ alloy has been found to enhance the phase stability of austenite, 6M and NM martensites while slightly decreasing ΔM. Optimized lattice calculations indicate that the introduction of Si reduces tetragonal distortion strain and volume changes during phase transformation. This can be predicted to reduce hysteresis in the phase transformation. These findings provide theoretical support for the design of new alloys.

Acknowledgments This work is financially supported by the National Natural Science Foundation of China (Grant No. 51771044), the Performance subsidy fund for Key Laboratory of Dielectric and Electrolyte Functional Material Hebei (No. 22567627H).

Conflict of Interest The authors state that there are no conflicts of interest to disclose.

Reference

[1] Kainuma R, Imano Y, Ito W, Sutou Y, Morito H, Okamoto S, Kitakami O, Oikawa K, Fujita A, Kanomata T, Ishida K. Magnetic-field-induced shape recovery by reverse phase transformation. Nature. 2006;439(7079):957-960.

[2] Monroe JA, Karaman I, Basaran B, Ito W, Umetsu RY, Kainuma R, Koyama K, Chumlyakov YI. Direct measurement of large reversible magnetic-field-induced strain in Ni-Co-Mn-In metamagnetic shape memory alloys. Acta Mater. 2012;60(20):6883-6891.

[3] Chabri T, Awasthi AM, Ghosh KC, Venimadhav A, Nath TK. Temperature and magnetic field dependent martensite transformation in Al doped Ni-Mn-Sn disorder alloys and its effects on magnetoresistance and magnetocaloric effect near room temperature. Mater. Res. Express. 2018;5(8):086511.

[4] Huang L, Cong DY, Ma L, Nie ZH, Wang MG, Wang ZL, Suo HL, Ren Y, Wang YD. Large magnetic entropy change and magnetoresistance in a $Ni_{41}Co_9Mn_{40}Sn_{10}$ magnetic shape memory alloy. J. Alloys Compd. 2015;647:1081-1085.

[5] Samanta T, Saleheen AU, Lepkowski DL, Shankar A, Dubenko I, Quetz A, Khan M, Ali N, Stadler S. Asymmetric switchinglike behavior in the magnetoresistance at low fields in bulk

metamagnetic Heusler alloys. Phys. Rev. B. 2014;90(6):064412.

[6] Liu J, Gottschall1 T, Skokov KP, Moore JD, Gutfleisch O. Giant magnetocaloric effect driven by structural transitions. Nat. Mater. 2012;11(7):620-626.

[7] Krenke T, Duman E, Acet M, Wassermann EF, Moya X, Mañosa L, Planes A. Inverse magnetocaloric effect in ferromagnetic Ni-Mn-Sn alloys. Nat. Mater. 2005;4(6):450-454.

[8] Singh S, Caron L, D'Souza SW, Fichtner T, Porcari G, Fabbrici S, Shekhar C, Chadov S, Solzi M, Felser C. Large Magnetization and Reversible Magnetocaloric Effect at the Second-Order Magnetic Transition in Heusler Materials. Adv. Mater. 2016;28(17):3321-3325.

[9] Zheng HX, Wang W, Xue SC, Zhai QJ, Frenzel J, Luo ZP. Composition-dependent crystal structure and martensitic transformation in Heusler Ni-Mn-Sn alloys. Acta Mater. 2013;61(12):4648-4656.

[10] Hobza A, Patrick CL, Ullakko K, Rafla N, Lindquist P, Müllner P. Sensing strain with Ni-Mn-Ga. Sensors Actuat A-Phys. 2018;269:137-144.

[11] Chiu WT, Sratong-on P, Tahara M, Chernenko V , Hosoda H. Large magnetostrains of Ni-Mn-Ga/silicone composite containing system of oriented 5M and 7M martensitic particles. Scr. Mater. 2022;207:114265.

[12] Yu SY, Ma L, Liu GD, Liu ZH, Chen JL, Cao ZX, Wu GH, Zhang B, Zhang XX. Magnetic field-induced martensitic transformation and large magnetoresistance in NiCoMnSb alloys. Appl. Phys. Lett. 2007;90:242501.

[13] Modak Rajkumar, Raja M. Manivel, Srinivasan A. Enhanced magneto-caloric effect upon Co substitution in Ni-Mn-Sn thin films. J. Magn. Magn. Mater. 2018;448:146-152.

[14] Miyakawa T, Ito T, Xu X, Omori T, Kainuma R. Martensitic transformation near room temperature and hysteresis in $(Ni\text{-}Co)_{50}$-Mn-Sn metamagnetic shape memory alloys. J. Alloys Comp. 2022;913:165136.

[15] Li ZB, Li ZZ, Yang JJ, Yang B, Zhao X, Zuo L. Large room temperature adiabatic temperature variation in a $Ni_{40}Co_8Mn_{42}Sn_{10}$ polycrystalline alloy. Intermetallics. 2018;100:57-62.

[16] Zhang GY, Li D, Liu C, Li ZB, Yang B, Yan HL, Zhao X, Zuo L. Giant low-field actuated caloric effects in a textured $Ni_{43}Mn_{47}Sn_{10}$ alloy. Scr. Mater. 2021;201:113947.

[17] Chen F, Śanchez Llamazares JL, Śanchez-Valdes CF, Müllner P, Tong YX, Li L. Influence of γ phase on the magnetostructural transition and magnetocaloric properties of $Ni_{38}Co_{12}Mn_{41}Sn_9$ melt-spun ribbons. J. Magn. Magn. Mater. 2023;579:170900.

[18] Nayak AK, Suresh KG, Nigam AK, Coelho AA, Gama S. Pressure induced magnetic and magnetocaloric properties in NiCoMnSb Heusler alloy. J. Appl. Phys. 2009;106:053901.

[19] Lázpita P, Ĺvov VA, Fernández JR, Barandiaran JM, Chernenko VA. Combined effect of magnetic field and hydrostatic pressure on the transitions exhibited by Ni-Mn-In metamagnetic shape memory alloy. Acta Mater. 2020;193:1-9.

[20] Ghosh S, Sen S, Mandal K. Effect of Si Doping on Magnetic and Magnetocaloric Properties of Ni-Co-Mn-Sn Alloys. IEEE. T. Magn. 2018;54(11):1-5.

[21] Maziarz W, Czaja P, Wójcik A, Wańkowicz K, Cesari E, Dutkiewicz J. Microstructure and martensitic transformation in $Ni_{48}Mn_{39.5}Sn_{12.5-x}Si_x$ metamagnetic Heusler alloy ribbons. Int. J. Mater. Res. 2015;106(7):711-718.

[22] Li FQ, Qu YH, Yan HL, Chen Z, Cong DY, Sun XM, Li SH, Wang YD. Giant tensile superelasticity originating from two-step phase transformation in a Ni-Mn-Sn-Fe magnetic microwire. Appl. Phys. Lett. 2018;113(11):112402.

[23] Koyama K, Watanabe K, Kanomata T, Kainuma R, Oikawa K, Ishida K. Observation of field-induced reverse transformation in ferromagnetic shape memory alloy $Ni_{50}Mn_{36}Sn_{14}$. Appl. Phys. Lett. 2016;88(13):132505.

[24] Zhang XX, Zhang HH, Qian MF, Geng L. Enhanced magnetocaloric effect in Ni-Mn-Sn-Co alloys with two successive magnetostructural transformations. Sci. Rep. 2018;8(1):8235.

[25] Kresse G, Joubert D. From ultrasoft pseudopotentials to the projector augmented-wave method. Phys. Rev. B. 1999;59(3):1758-1775.

[26] Blöchl PE. Projector augmented-wave method. Phys. Rev. B. 1994;50(24):17953-17979.

[27] Kern G, Kresse G, Hafner J. Ab initio calculation of the lattice dynamics and phase diagram of boron nitride. Phys. Rev. B. 1999;59(13):8551-8559.

[28] Perdew JP, Burke K, Ernzerhof M. Generalized gradient approximation made simple. Phys. Rev. Lett. 1996;77(18):3865-3868.

[29] Yan HL, Zhang YD, Xu N, Senyshyn A, Brokmeier HG, Esling C, Zhao X, Zuo L. Crystal structure determination of incommensurate modulated martensite in Ni-Mn-In Heusler alloys. Acta Mater. 2015;88:375-388.

[30] Zhang Y, Bai J, Guan ZQ, Liang XZ, Li YS, Gu JL, Zhang YD, Esling C, Zhao X, Zuo L. Phase Stability, magnetic properties, and martensitic transformation of $Ni_{2-x}Mn_{1+x+y}Sn_{1-y}$ Heusler alloy with excess Mn by first-principles calculations. Acta. Metall. Sin-Engl. 2023;36(3):513-528.

[31] Li CM, Luo HB, Hu QM, Yang R, Johansson B, Vitos L. First-principles investigation of the

composition dependent properties of $Ni_{2+x}Mn_{1-x}Ga$ shape-memory alloys. Phys. Rev. B. 2010;82(2):024201.

[32] Liang XZ, Bai J, Guan ZQ, Gu JL, Yan HL, Zhang YD, Esling C, Zhao X, Zuo L. Revealing the role of site occupation in phase stability, magnetic and electronic properties of Ni-Mn-In alloys by ab initio approach. J. Mater. Sci. Technol. 2021;83:90-101.

[33] Li CM, Luo HB, Hu QM, Yang R, Johansson B, Vitos L. Site preference and elastic properties of Fe-, Co-, and Cu-doped Ni_2MnGa shape memory alloys from first principles. Phys. Rev. B. 2011;84(2):024206.

[34] Kundu A, Ghosh S, Ghosh S. Effect of Fe and Co substitution on martensitic stability, elastic, electronic and magnetic properties of Mn_2NiGa: insights from ab initio calculations. Phys. Rev. B. 2017;96(17):174107.

[35] Ghosh S, Levente V, Sanyal B. Structural and elastic properties of $Ni_{2+x}Mn_{1-x}Ga$ alloys. Phys. B. 2011;406(11):2240-2244.

[36] Zhang Y, Bai J, Guo KL, Xu JX, Gu JL, Morley N, Gao QZ, Zhang YD, Esling C, Zhao X, Zuo L. Unraveling magnetic properties and martensitic transformation in Mn-rich Ni-Mn-Sn alloys: first-principles calculations and experiments. Rare Metals. 2024;43(4):1769-1785.

[37] Chen XQ, Yang FJ, Lu X, Qin ZX. The way composition affects martensitic transformation temperatures of Ni-Mn-Ga Heusler alloys. Phys. Stat. Sol. (b). 2007;244(3):1047-1053.

[38] Banik S, Mukhopadhyay PK, Awasthi AM, Barman SR. Structural Studies on Mn Excess and Ga Deficient Ni-Mn-Ga. Adv. Mater. Res. 2008;52:109-114.

[39] Lanska N, Söderberg O, Sozinov A, Ge Y, UllakKo K, Lindroos VK. Composition and temperature dependence of the crystal structure of Ni-Mn-Ga alloys. J. Appl. Phys. 2004;95(12):8074-8078.

[40] Fujii S, Ishida S, Asano S. Electronic structure and lattice transformation in Ni_2MnGa and Co_2NbSn. J. Phys. Soc. Jpn. 1989;58(10):3657-3665.

[41] Lázpita P, Barandiarán JM, Gutiérrez J, Feuchtwanger J, Chernenko VA, Richard ML. Magnetic moment and chemical order in off-stoichiometric Ni-Mn-Ga ferromagnetic shape memory alloys. New. J. Phys. 2011;13(3):033039.

[42] Cui J, Chu YS, Famodu OO, Furuya Y, Hattrick-simpers J, James RD, Ludwig A, Thienhaus S, Wuttig M, Zhang ZY, Takeuchi I. Combinatorial search of thermoelastic shape-memory alloys

with extremely small hysteresis width. Nat. Mater. 2006;5(4):286-290.

[43] Yan HL, Liu HX, Zhao Y, Jia N, Bai J, Yang B, Li ZB, Zhang YD, Esling C, Zhao X, Zuo L. Impact of B alloying on ductility and phase transition in the Ni-Mn-based magnetic shape memory alloys: Insights from first-principles calculation. J. Mater. Sci. Technol. 2021;74:27-34.

[44] Li ZB, Jiang YW, Li ZZ, Valde´s CFS, Llamazares JLS, Yang B, Zhang YD, Esling C, Zhao X, Zuo L. Phase transition and magnetocaloric properties of $Mn_{50}Ni_{42-x}Co_xSn_8$ ($0 \leq x \leq 10$) melt-spun ribbons. IUCrJ. 2018;5:54-66.

[45] Yang JJ, Li ZB, Yang B, Yan HL, Cong DY, Zhao X, Zuo L. Effects of Co and Si co-doping on magnetostructural transformation and magnetocaloric effect in Ni-Mn-Sn based alloys. J. Alloys Comp. 2021;892:162190.